

# New Method of Analysis for Slender Columns



by Zdeněk P. Bažant, Luigi Cedolin, and Mazen R. Tabbara

*This paper presents a simple new method to calculate column-interaction diagrams, which takes into account slenderness effects. The method consists of a simple incremental-loading algorithm that traces the load-deflection curve at constant eccentricity of the axial load. The column failure is defined for design purposes as the peak of the diagram of axial load versus midlength bending moment at constant load eccentricity. The tangent modulus load is found to be approximately equal to the peak load of a column with load eccentricity 0.01 of the cross-sectional thickness and represents a lower bound for the maximum loads at still smaller eccentricities. Strain irreversibility at unloading can be taken into account but its effect is very small. The method is compared with the ACI moment magnification method and with the CEB model column method based on moment-curvature relations. The agreement with the CEB method is very close, but with respect to the ACI method there are large discrepancies.*

**Keywords:** columns (supports); failure; loads (forces); slenderness ratio; stress strain relationships; structural analysis; structural design; tangent modulus.

Although the design of reinforced columns for buckling is by now a well-researched and relatively well-understood subject, the state of the art is far from perfect. A variety of design methods are in use and the design recommendations of ACI<sup>1</sup> and CEB<sup>2,3</sup> differ considerably. The design methods introduce simplifications which might prove too crude, causing the safety margins for various situations to be far from uniform. The objective of the present paper is to show a new method of analysis distinguished by simplicity.

## PRELIMINARIES: STRESS-STRAIN RELATIONS

For columns, it is usually sufficient to use a uniaxial stress-strain diagram, the typical form of which is sketched in Fig. 1(a). The use of the smooth descending (strain-softening) portion of the  $\sigma(\epsilon)$  diagram implies that strain-localization instabilities do not occur. This appears to be a reasonable assumption for columns, as long as the diagram of load  $P$  versus load-point displacement  $u_1$  is rising. In this study we are interested only in such behavior. However, note that strain-softening behavior is difficult to measure since strain localization occurs in a uniaxial test specimen right after the peak. In view of these difficulties, the practice for concrete has been to assume a stress-strain diagram terminating with a sudden drop.

Although other formulas might be preferable, in this study we will use only the formulas from design recommendations or codes. The CEB Model Code<sup>2</sup> specifies [Curve 1, Fig. 1(b)]

$$\sigma_c = \begin{cases} (2-\xi)\xi f_p & \xi \leq 1 \\ f_p & 1 \leq \xi \leq 1.75 \\ 0 & \xi \geq 1.75 \end{cases} \quad (1)$$

where  $\xi = \epsilon_c/\epsilon_c^p$ ,  $f_p$  = peak stress, and  $\epsilon_c^p$  = strain at peak stress;  $\epsilon_c^p = 0.002$ . The CEB Model Code Predraft<sup>3</sup> recommends a smooth descending stress-strain diagram without any plateau, given as follows [Curve 2, Fig. 1(b)]:

$$\sigma_c = \begin{cases} f_p \frac{M\xi - \xi^2}{1 + (M-2)\xi} & \text{for } \xi \leq \xi_u \\ f_p \left[ \left( \frac{N}{\xi_u} - \frac{2}{\xi_u^2} \right) \xi^2 + \left( \frac{4}{\xi_u} - N \right) \xi \right]^{-1} & \text{for } \xi > \xi_u \end{cases} \quad (2)$$

in which  $\epsilon_c^p = 0.0022$ ,  $E_c^0$  = initial modulus =  $0.142 \times 10^4 (f_p/0.142)^{1/3}$ ,  $E_c^p = f_p/\epsilon_c^p$ ,  $\xi_u = \epsilon_c^u/\epsilon_c^p$ ,  $\epsilon_c^u$  = post-peak strain at  $\sigma_c^u = 0.5f_p$ ,  $M = E_c^0/E_c^p$ , and  $N = 4[\xi_u^2(M-2) + 2\xi_u - M]/[\xi_u(M-2) + 1]^2$ . In calculating the initial modulus,  $f_p$  should be expressed in kips/in.<sup>2</sup>.

The stress-strain curve for steel reinforcement is given by

$$\sigma_s = \begin{cases} E_s^0 \epsilon_s & \epsilon_s \leq \epsilon_s' \\ f_y & \epsilon_s > \epsilon_s' \end{cases} \quad (3)$$

where  $E_s^0$  = initial modulus,  $f_y$  = yield stress, and  $\epsilon_s'$  = strain at the start of yielding.

ACI Structural Journal, V. 88, No. 4, July-August 1991.  
Received Mar. 5, 1990, and reviewed under Institute publication policies.  
Copyright © 1991, American Concrete Institute. All rights reserved, including the making of copies unless permission is obtained from the copyright proprietors. Pertinent discussion will be published in the May-June 1992 ACI Structural Journal if received by Jan. 1, 1992.

Zdeněk P. Bažant, F.A.C.I., is Walter P. Murphy Professor of Civil Engineering at Northwestern University, Evanston, Ill., where he served as Founding Director of the Center for Concrete and Geomaterials. He is a registered structural engineer, a consultant to Argonne National Laboratory, and editor-in-chief of the ASCE Journal of Engineering Mechanics. He is chairman of ACI Committee 446, Fracture Mechanics; a member of ACI Committees 209, Creep and Shrinkage of Concrete, and 348, Structural Safety; chairman of RILEM Committee TC 107 on Creep, of ASCE-EMD Programs Committee, and of SMIRT Division of Concrete and Nonmetallic Materials; and a member of the Board of Directors of the Society of Engineering Science. Currently he conducts research at the Technical University in Munich under the Humboldt Award of U.S. Senior Scientist.

ACI member Luigi Cedolin is a professor of structural engineering at the Politecnico di Milano, Italy. He has been Senior Visiting Scientist to Cornell University and Northwestern University and a member of the CEB Task Group on Concrete under Multiaxial Stress States. He is a member of ACI Committee 446, Fracture Mechanics, of the ASCE Committee on Finite Element Analysis of Reinforced Concrete Structures, and of RILEM Committees on Fracture Mechanics and Mathematical Modeling of Creep and Shrinkage of Concrete.

ACI member Mazen R. Tabbara is a Post-Doctoral Fellow at Northwestern University, Evanston, Illinois. His research interests include constitutive models for nonlinear materials, fracture mechanics, and finite element applications.

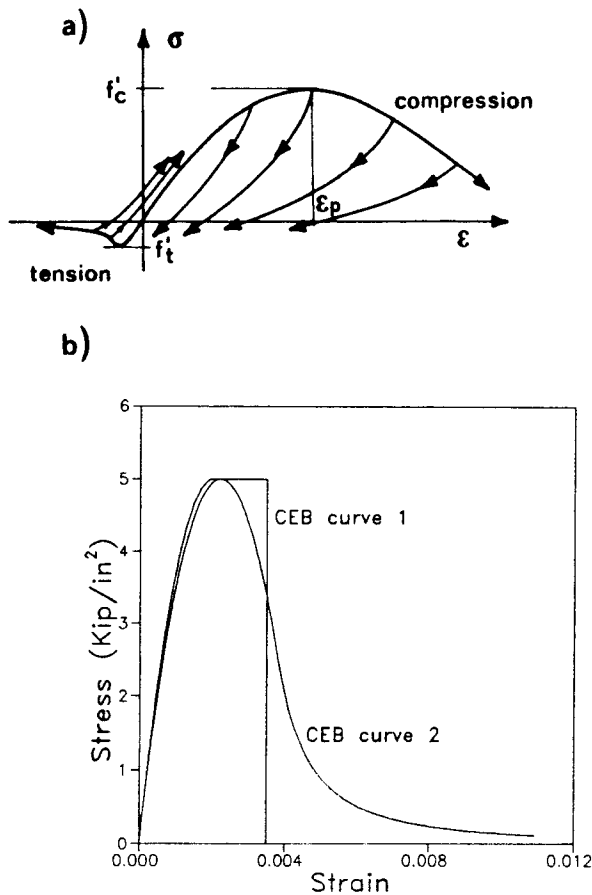


Fig. 1 — (a) Typical uniaxial stress-strain curve for concrete; (b) stress-strain curves recommended by CEB code.

It should be emphasized that the post-peak strain-softening portion of the effective stress-strain relation depends on many factors not normally considered in design. This is due to strain localization,<sup>4</sup> which occurs in softening materials. Depending on the degree of localization of strain, the average post-peak slope can be mild or steep (or even snapback can occur). Conse-

quently, the steepness of the post-peak stress-strain relation must be expected to depend on the axial steel, the transverse steel (ties or spirals), the shape and size of the cross section, etc. As long as these factors are neglected, it makes little sense to argue whether one or another formula for the  $\sigma_c(\epsilon_c)$  curve is better. The fact that laboratory tests of a standard specimen give a certain curve is not very relevant. One would need actually to calculate the localization of the softening zone in the column to profit from a sophisticated stress-strain relation (Chapter 13 of Reference 4). In this light, Eq. (2) seems to be unjustifiably complicated. A short formula such as  $\sigma_c = E_c^0 \epsilon_c \exp(-k\epsilon_c^2)$ , with  $k = \text{constant}$ , might be just as good or just as poor.

## COLUMN-INTERACTION DIAGRAMS

The ultimate compressive force and the ultimate bending moment for a concrete column cross section are related by an interaction diagram (or failure surface), whose typical shape is shown in Fig. 2(b). It may be helpful to discuss first how this diagram is defined. To avoid second-order effects, one considers a short element (slice)  $\Delta x$  of the column. The element is subjected to axial force  $P$  applied at constant eccentricity  $e$  [Fig. 2(a)]. The load-point displacement  $u_1$  is increased in small steps, and the corresponding values of  $P$  are calculated from equilibrium conditions and the stress-strain laws of concrete and steel, assuming the cross sections to remain plane. If the curve  $P(u_1)$  is rising, the beam element is stable, i.e., no failure. If the curve is descending, the column element is unstable under load control. The critical point (or limit) of stability, i.e., the failure point, is obtained as the peak-load point  $P_{max}$  [Fig. 2(c)]. Thus the interaction diagram (at controlled load) should be defined and calculated as the collection of the peak-load points of all the curves  $P(u_1)$  obtained for all the eccentricities  $e$ .

In the practical engineering literature, this theoretically consistent (stability-based) definition of failure is normally not adhered to. Rather, failure is assumed to occur when the maximum strain of concrete or steel reaches a certain specified limit, which is selected empirically. However, if calculations beyond this limit (based on a realistic constitutive law) would indicate a further increase of load [Fig. 2(d)], this limit cannot really be a failure state. Furthermore, if calculations indicate that the load at this limit is already decreasing, then again this cannot be a failure state, since failure must have occurred earlier.

Consider now a column under increasing axial load  $P$  with constant end eccentricity  $e$  [Fig. 3(d)]. The path followed by axial load  $P$  and bending moment  $M$  at column midlength is shown in Fig. 3(e). If second-order effects are absent (as in very short columns), the cross section undergoes proportional loading, and its state follows the radial ray  $\bar{O}1$  (of slope  $e = M/P$ ), reaching a maximum at Point 1 of the cross-sectional interaction diagram. For slender columns, however, the midlength deflection  $w_1$  causes the path to deviate from the radial ray downward (Path  $\bar{O}2$ ). The larger the col-

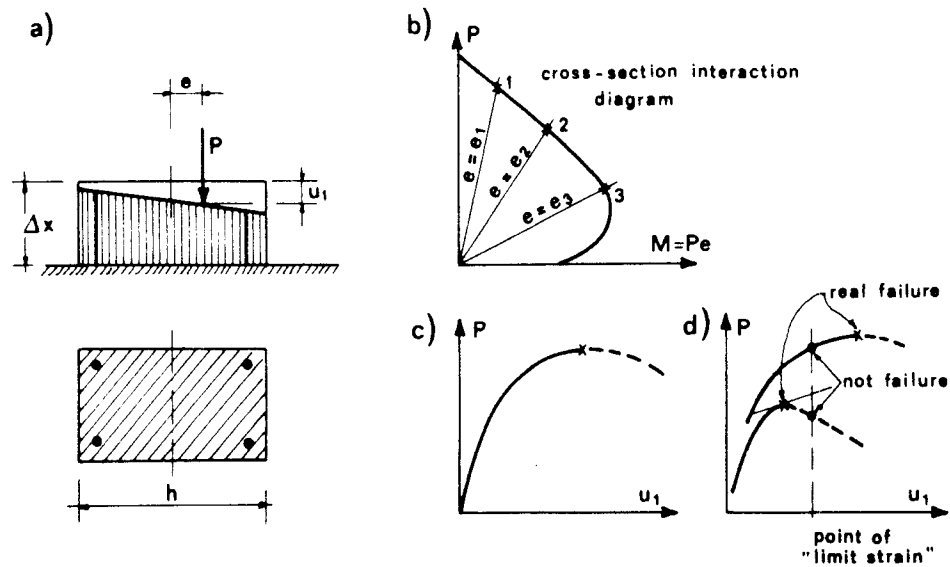


Fig. 2 — (a) Short element along the length of the column; (b) typical interaction diagram for columns; (c) load-deflection curve with failure occurring at peak load; (d) real failure versus "limit strain" state

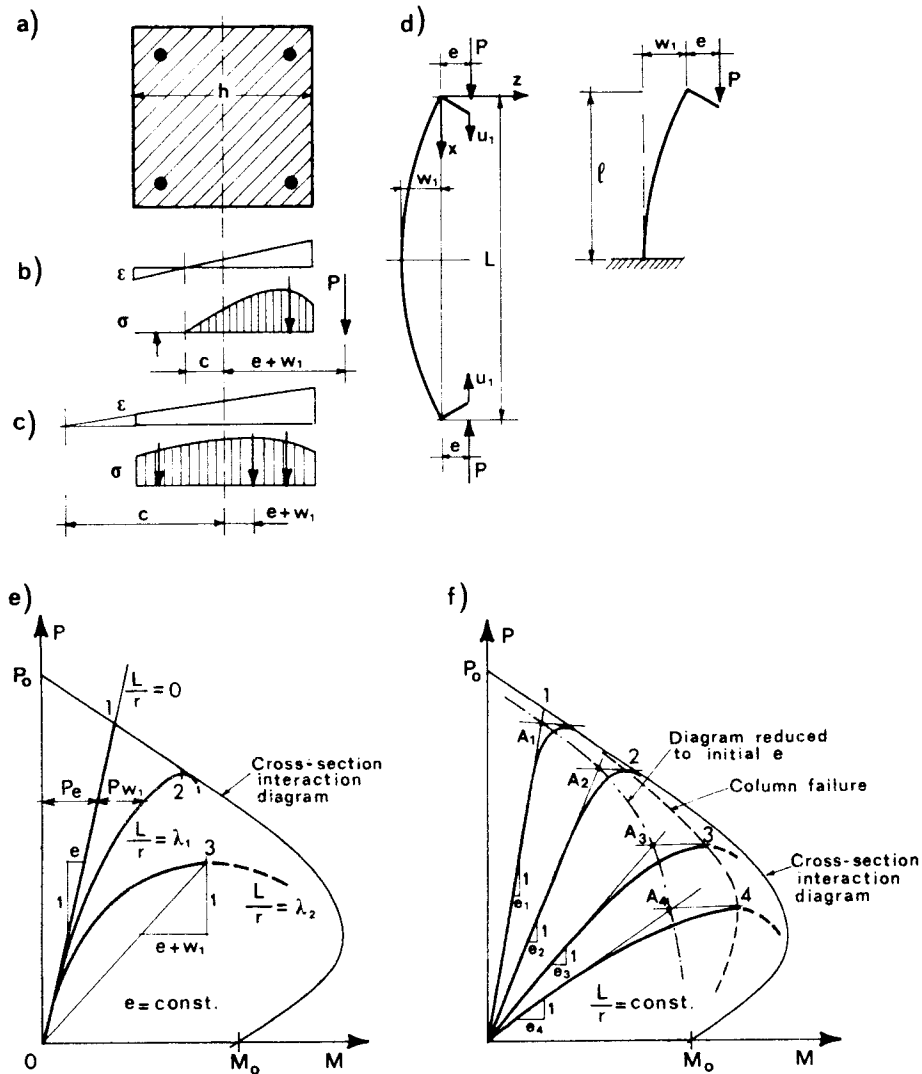


Fig. 3 — (a) Cross section of column used in analysis: Strain and stress distribution along the column cross section for (b)  $c < h/2$  and (c)  $c > h/2$ ; (d) configuration of the representative column used in the analysis; (e) load-versus-moment diagram for various slenderness ratios but the same eccentricity; (f) load-versus-moment diagram for various eccentricities but the same slenderness ratio

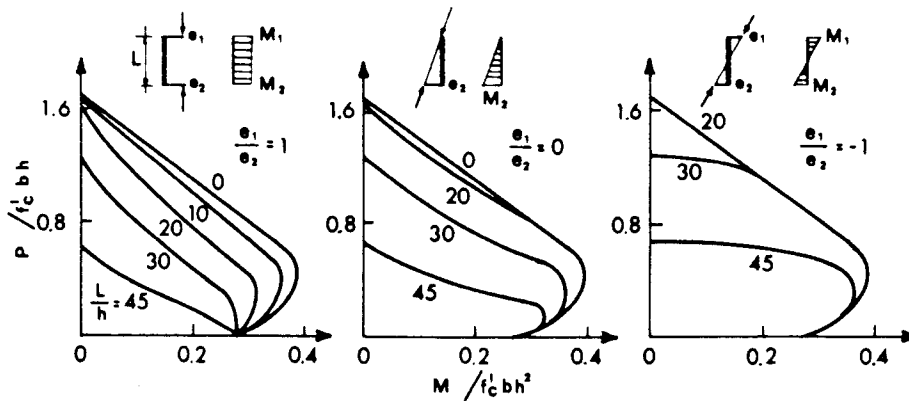


Fig. 4 — Reduced interaction diagrams for three different ratios of end eccentricities, adapted from MacGregor<sup>7</sup>

umn slenderness  $\lambda$ , the greater is the deviation ( $\lambda = L/r$ , where  $L =$  effective column length and  $r =$  radius of gyration).

For not-too-slender columns, the failure (peak) occurs at points rather close to (but still inside) the cross-sectional interaction diagram (Path  $\overline{02}$ ). Such behavior corresponds to what is called cross section failure. For very slender columns, on the other hand, the failure occurs well within the cross-sectional interaction diagram (Path  $\overline{03}$ ), because of pronounced second-order effects. This corresponds to what is called the stability failure.

Fig. 3(f) compares the  $P(M)$  paths at constant  $e$  for columns of the same  $\lambda$  but different eccentricities  $e_1$ . Connecting the failure points, such as 1, 2, and 3, yields the interaction diagram  $P(M)$  modified for second-order effects. Projecting each failure point horizontally onto Point  $A_1$  on the radial line of slope  $e_1$ , one obtains the reduced interaction diagram. Fig. 4, adapted from MacGregor, Breen, and Pfrang,<sup>5</sup> shows the reduced interaction diagrams for three different ratios of the end moments and for various values of the ratio  $L/h$ . These diagrams, as well as the actual column-interaction diagrams [Curves  $\overline{234}$  in Fig. 3(f)], differ for different column slendernesses.

### PROPOSED METHOD FOR INTERACTION DIAGRAMS

For simplicity, it is customary to assume that the deflected curve is sinusoidal, i.e.,  $w = -w_1 \sin(\pi x/L)$ , where  $L =$  effective length of the column [Fig. 3(d)]. The equilibrium condition and the moment-curvature relation can then be satisfied exactly only at the midlength of the column, and so our solution will be only approximate. The curvature at midlength is  $\kappa = \pi^2 w_1/L^2$ , from which  $w_1 = L^2 \kappa/\pi^2$ . By equilibrium, the second-order bending moment is  $M_{II} = Pw_1$ , or

$$M_{II} = Pk_{II}\kappa, \quad k_{II} = L^2/\pi^2 \quad (4)$$

(In reality, coefficient  $k_{II}$  must be less than  $L^2/\pi^2$  because nonlinear behavior tends to produce a sharper, more pointed curve at midspan than a sine curve.) The total moment at midlength is  $M = M_I + M_{II}$ , where  $M_I$

$= Pe =$  first-order (primary) bending moment, which is due to eccentricity  $e$  of load  $P$  at both column ends. The maximum of the response curve  $P(M)$  at constant  $e$  represents the failure point under load control. Consequently, the collection of all these maxima for various  $e$  determines the failure envelope of the column. This can be proven as follows.

The failure point under load control is characterized by the condition  $dP/du_1 = 0$ . For a sinusoidal column shape, the magnitude of the rotation at the column end is  $\theta_1 = w_1\pi/L$ . Thus the load-point displacement is  $u_1 = 2\theta_1 e + \int_0^L (w'^2/2) dx = 2\pi e w_1/L + \pi^2 w_1^2/4L$ , in which  $w_1 = L^2 \kappa/\pi^2$  and the axial shortening of the column axis is neglected. So the sinusoidal approximation gives

$$u_1 = \frac{2eL}{\pi} \kappa + \frac{L^3}{4\pi^2} \kappa^2 \quad (5)$$

The column is stable if  $dP/du_1 > 0$ . It fails when the response first satisfies the condition  $dP/du_1 \leq 0$ , i.e.

$$\frac{dP}{du_1} = \frac{dP}{dM} \frac{dM}{d\kappa} \frac{d\kappa}{du_1} \leq 0 \quad (6)$$

If the slope  $dP/du_1$  varies continuously, then the failure condition is  $dP/du_1 = 0$ . Differentiation of Eq. (5) shows that  $d\kappa/du_1 \geq 0$  (since  $\kappa \geq 0$ ,  $e > 0$ ). It is possible that  $dM/d\kappa$  at failure is either nonpositive or positive. If  $dM/d\kappa \leq 0$ , the cross section fails even without the second-order (slenderness) effect. Thus this type of failure, which occurs at Point 1 of Fig. 5(a), is obtained for zero slenderness ( $L = 0$ ), and in this case,  $dP/dM \neq 0$  for the points on the cross-sectional interaction diagram. But for  $L > 0$  we have  $dM/d\kappa > 0$ . So the column fails as soon as  $dP/dM \leq 0$ . This proves that the peak point of the  $P(M)$  diagram at constant  $e$  represents failure.

If the slope  $dP/dM$  at constant  $e$  varies continuously, then the column fails when  $dP/dM = 0$ ; in that case, the response curves  $\overline{02}$ ,  $\overline{03}$ , and  $\overline{04}$  in Fig. 5(a) must intersect the column interaction diagram  $P(M)$  horizontally. If the slope changes discontinuously, then the intersection with the column interaction diagram [Fig. 5(b)] is characterized by the fact that  $dP/dM$  is

positive on the left and nonpositive on the right of the intersection. This situation may arise if the column fails when the steel bars begin to yield, provided that the steel is assumed to behave as elastic-perfectly plastic. When a change of slope  $d\sigma_s/d\epsilon_s$  due to the start of yielding of steel causes a sudden change in the slope  $dP/dM$ , the peak point of the  $P(M)$  curve, representing the failure point, may lie exactly on the cross-sectional interaction diagram (see Fig 5(b)). A sudden change in the slope  $d\sigma_c/d\epsilon_c$  of the  $\sigma_c(\epsilon_c)$  diagram of concrete, on the contrary, cannot cause a sudden change of slope  $dP/dM$  because changes of  $d\sigma_c/d\epsilon_c$  cannot be simultaneous (for  $\kappa \neq 0$ ) in a finite (nonvanishing) portion of the cross section.

The critical cross section at column midlength is subdivided into many thin layers representing the concrete area. The steel area at each corner [Fig. 3(a)] is considered to be concentrated at a point. Knowing the values of the curvature  $\kappa$  and the distance  $c$  from the beam axis to the neutral axis [Fig. 3(b) and (c)], one has  $\epsilon = -\kappa(z + c)$ . So the given  $\sigma(\epsilon)$  diagram of concrete and steel for either loading or unloading can be used to evaluate the stress at the center point of every layer. From these stress values one obtains the resultants  $P = P(\kappa, c)$  and  $M = M(\kappa, c)$ .

To determine the curve  $P(M)$  at increasing column deflection and constant eccentricity  $e$  at the column ends, the following algorithm is proposed. One chooses an increasing sequence on  $\kappa$ -values. For each  $\kappa$ -value, one has  $w_1 = k_{11}\kappa$ . So one needs to solve  $c$  from the equilibrium equation

$$M(\kappa, c) - (e + w_1)P(\kappa, c) = 0 \quad (7)$$

in which  $M$  and  $P$  are calculated as the resultants of the stresses in all the layers corresponding to strains  $\epsilon = -\kappa(z + c)$ . Eq. (7) (which insures equilibrium only at column midlength) is a nonlinear equation which is quite easy to solve by iteration using a computer library subroutine. The convergence is very fast if the solution of  $c$  for the preceding  $\kappa$ -value is used as the initial estimate of  $c$  for the next  $\kappa$ -value in the loading sequence.

From the  $c$ -value obtained and the value of  $\kappa$ , one can then evaluate  $P(\kappa, c)$  and  $M(\kappa, c)$ , which defines a point on the  $P(M)$  curve at constant  $e$ . However, before calculating  $P$  and  $M$  from  $\kappa$  and  $c$ , the current strain value in the centroid of each layer has to be compared with the strain value at the previous load level, and if unloading is detected, then the proper  $\sigma(\epsilon)$  curve for unloading should be considered for that layer. In our case, unloading is taken as a straight line parallel to the initial tangent of the  $\sigma(\epsilon)$  curve.

#### TANGENT AND REDUCED MODULUS LOADS

In general, the tangent modulus load  $P_t$  and the reduced modulus load  $P_r$  are important characteristics in the theory of inelastic columns.<sup>4,6</sup> In the present context, these load values give an approximate lower

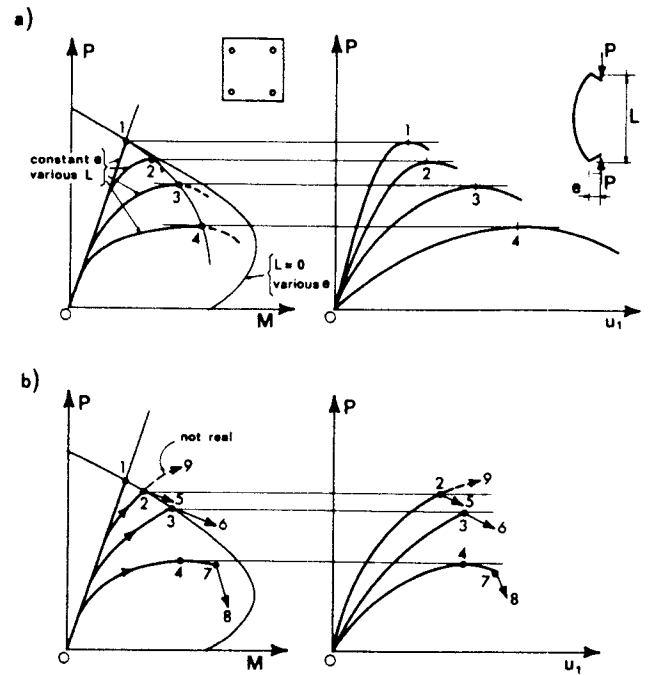


Fig. 5 — (a) Load-versus-moment and load-versus-deflection diagrams with a continuously decreasing slope; (b) Load-versus-moment and load-versus-deflection diagram with discontinuous slope

bound and an upper bound for  $P_{max}$  of a column with a small  $e$ . For a symmetric cross section,  $P_t$  is the Euler's critical load based on the tangential moduli in the undeflected initial state of a perfect column ( $e = 0$ )

$$P_t = \frac{\pi^2}{L^2} (E'_c I_c + E'_s I_s) \quad (8)$$

This must be equal to the axial force resultant

$$P_t = (\sigma_c A_c + \sigma_s A_s) \quad (9)$$

Subscripts  $c$  and  $s$  stand for concrete and for steel, respectively,  $A$  is the cross-sectional area, and  $I$  is the moment of inertia of the cross section about the centroidal axis. The values of the tangential moduli  $E'_c$  and  $E'_s$ , as well as the stress values  $\sigma_c$  and  $\sigma_s$ , depend on the axial strain  $\epsilon = \epsilon_c = \epsilon_s$ . Thus, equating the expressions in Eq. (8) and (9), one obtains a single nonlinear equation with  $\epsilon$  as a single unknown, which can be easily solved by an iterative procedure.

To find an expression for  $P_r$  for the rectangular cross section in Fig. 3(a), consider a small variation in curvature  $\delta\kappa$ . The corresponding  $\delta M$  is

$$\delta M = \left\{ \frac{1}{3} b (E'_c h_l^3 + E'_s h_u^3) + \frac{1}{2} A_s [E'_s (h_l - h_u)^2 + E'_c (h_u - h_c)^2] \right\} \delta\kappa \quad (10)$$

where  $b$  = width of the cross section,  $h_c$  = concrete cover,  $h_l$  = the portion of  $h$  that undergoes loading, and  $h_u = h - h_l$  = the portion of  $h$  that undergoes

unloading. Eq. (10) assumes that the unloading, in both concrete and steel, follows the initial slope. Eq. (10) can be rewritten in a more familiar way using the effective bending stiffness  $\overline{EI}$

$$\overline{EI} = \frac{\delta M}{\delta \kappa} = \Phi_c E_c^0 I_c + \Phi_s E_s I_s \quad (11)$$

where

$$\Phi_c E_c^0 I_c = \frac{1}{3} b (E_c' h_L^3 + E_c^0 h_U^3) \quad (12)$$

$$\Phi_s E_s^0 I_s = \frac{1}{2} A_s [E_s^0 (h_L - h_c)^2 + E_s^0 (h_U - h_c)^2] \quad (13)$$

$P_r$  may now be expressed as the Euler load of a perfect column ( $e = 0$ ) with bending stiffness  $\overline{EI}$

$$P_r = \frac{\pi^2}{L^2} (\Phi_c E_c^0 I_c + \Phi_s E_s^0 I_s) \quad (14)$$

This must be equal to the axial-load resultant in the undeflected state

$$P_r = (\sigma_c A_c + \sigma_s A_s) \quad (15)$$

The solution of Eq. (14) and (15) also requires an iterative procedure because  $\Phi_c$  and  $\Phi_s$  depend on the tangential moduli which in turn depend on the axial strain. Setting the expressions in Eq. (14) and (15) equal, one gets a nonlinear equation with two unknowns,  $\epsilon$  and  $h_L$ . A second equation is obtained from the condition  $\delta P = 0$ , which defines the reduced modulus load. This condition yields a quadratic equation in terms of  $h_L$

$$h_L^2 b (E_c' - E_c^0) + h_L (2hbE_c^0 + A_s E_s' + A_s E_s^0) - bE_c^0 h^2 - A_s E_s^0 h + h_c A_s (E_s^0 - E_s') = 0 \quad (16)$$

The iterative solution starts by assuming a strain value in the cross section. The corresponding moduli and stresses can then be calculated from the given stress-strain curves. The next step is to calculate  $h_L$  from Eq. (16) and substitute its value in Eq. (12) and (13) to find  $\Phi_c$  and  $\Phi_s$ . It is now possible to check Eq. (14) and (15); if they are satisfied,  $P_r$  is then calculated, and if not then another value of strain is selected and the procedure is repeated until Eq. (14) and (15) are satisfied.

### NUMERICAL EXAMPLE

Next, consider concrete columns of square cross section with side length  $h = 22$  in. (Fig. 3) and various slendernesses  $l/r$  where  $r = h/\sqrt{12}$ . The concrete is assumed to follow the curve given in Eq. (2) with  $f_p = f_c' = 5000$  psi for compression while having no stiffness in tension. The reinforcement is symmetric, with a steel ratio of  $\rho_s = 0.03$  and a concrete cover such that the bar centroid is 3 in. from the surface. The stress-strain relation for steel is given by Eq. (3) with  $E_s = 29 \times 10^6$  psi and  $f_s = 60,000$  psi, for both compression and ten-

sion. Unloading in both materials, concrete and steel, is assumed to be along a straight line parallel to the initial slope of the stress-strain curve.

The calculated response curves  $P(M)$  at constant  $e$  (Fig. 6) confirm that the peak-load point occurs always within the cross-sectional interaction diagram, rather than on it. In textbooks, it has been widely assumed that, for small  $e$ , the response curve intersects the cross-sectional interaction diagram with a positive slope; but this is not the case. For columns of medium slenderness ( $l/r \approx 70$ ), the peaks of the  $P(M)$  curves (i.e., the failure points) lie rather close to the cross-sectional interaction diagram—this is true for small as well as large eccentricities  $e$ . On the other hand, for very slender columns ( $l/r \approx 100$ ), these peaks are quite remote from the interaction diagram for all eccentricities except the very large ones ( $e > 0.3h$ ). The corresponding diagrams  $P(u_1)$ , which of course have the same peak  $P$ -values as the diagrams  $P(M)$ , are shown on the right.

Using Eq. (8) and (14), it is possible to calculate  $P_r$  and  $P_r$  for this example. The results are shown in Fig. 6. As expected,  $P_r < P_{max} < P_r$  for small eccentricities ( $e \leq 0.01h$ ). This condition is satisfied as long as the steel is not yielded; otherwise,  $P_{max}$  admits only an upper bound  $P_r$ , calculated by setting  $\epsilon_s = \epsilon_c = \epsilon_c'$ . It may also be concluded that  $P_r$  gives a good estimate of  $P_{max}$  for  $e = 0.01h$  as long as the steel does not yield. Note that this value of  $e$  is much less than the minimum eccentricity according to the ACI Building Code,<sup>1</sup> which is  $e_{min} = 0.6 + 0.03h = 1.26$  in. =  $0.06h$ . For this eccentricity,  $P_{max}$  is much less than  $P_r$  (see Fig. 6), which means the ACI Building Code is very conservative for small eccentricities.

Fig. 7 shows the effect of varying the column slenderness at various eccentricities. Note that the trend of the interaction envelope continues smoothly into the tensile side ( $P < 0$ ), which means that eccentricity weakens the tensile capacity of a beam. Also note that the second-order effect strengthens a column under tension since it deflects the loading path again below (but to the left of) the straight radial path for zero slenderness (calculated as the maximum value of  $P$  for various  $e/h$ ).

Fig 8 compares the response curves obtained with the  $\sigma_c(\epsilon_c)$  relations in Eq. (1) and (2). The curves practically coincide up to  $P_{max}$ , after which, however, the curves obtained with Eq. (1) tend to be higher and reach higher values of  $M$ . On the curves obtained with Eq. (1), the point at which the strain in concrete reaches 0.0035 has been marked; this point corresponds to the limit strain in concrete according to the CEB code.

Fig. 9 shows the effect of ignoring concrete and steel unloading [i.e., the virgin  $\sigma(\epsilon)$  curve is retraced when unloading occurs]. During loading at constant  $P$ , unloading typically occurs as the neutral axis moves into the previously compressed portion of the cross section [See later Fig. 14(h)]. This effect, however, is seen to be negligible, at least up to the peak point of the column response. The reason is that the loading-unloading reversal occurs near the neutral axis where stress has little

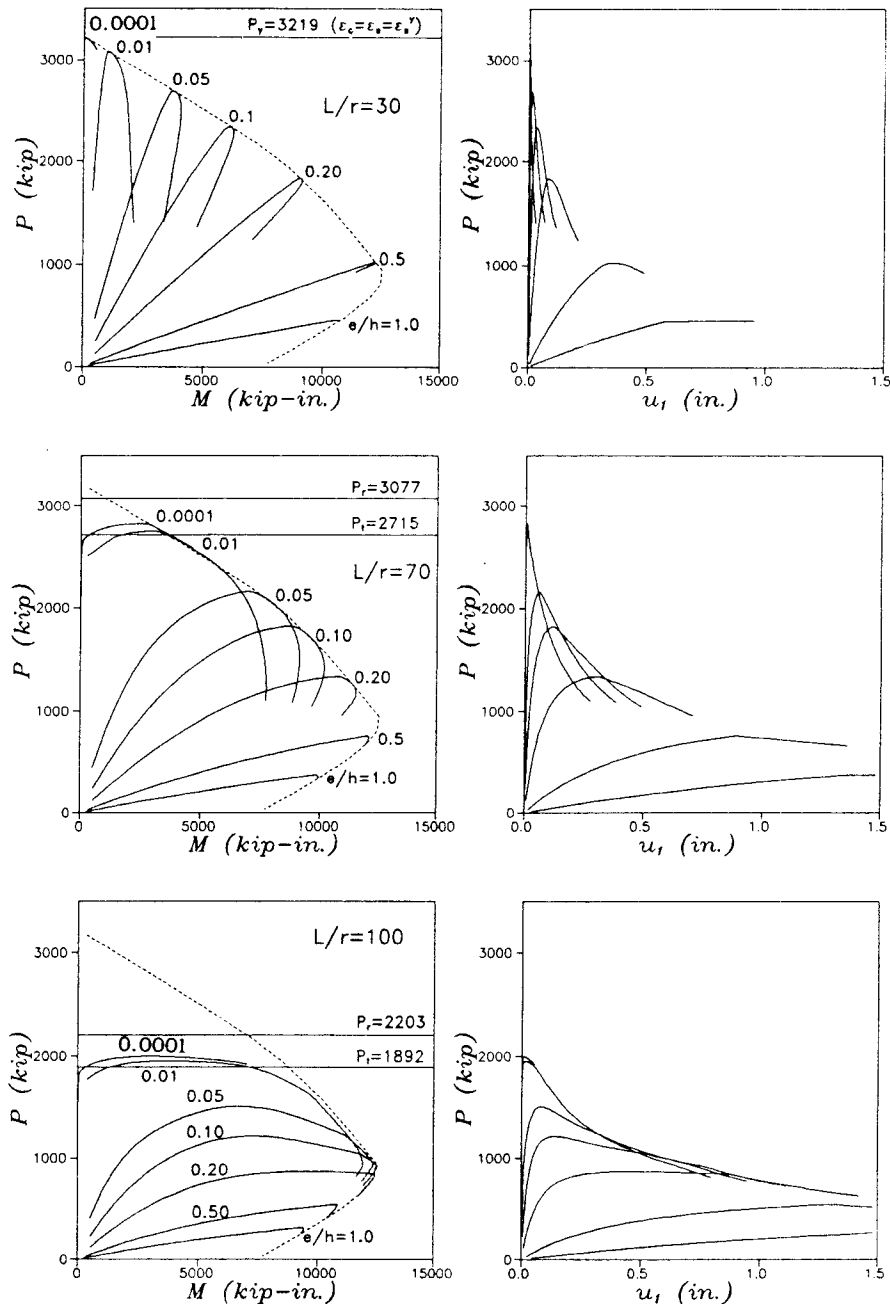


Fig. 6 — Calculated response curves at constant  $e$  for  $L/r = 30, 70,$  and  $100$  with Shanley's tangent modulus load  $P_t$  shown as a horizontal line

effect on  $M$ ; furthermore, it occurs at low strain levels at which the stress-strain diagram for loading is close to that for unloading.

Fig. 10 shows the column failure envelope and the reduced failure envelope in terms of primary bending moments. As it can be seen, the reduced failure envelope is close to both the column and the cross-sectional failure envelopes for low slendernesses ( $L/r \approx 30$ ), but it moves farther apart for higher slendernesses.

#### COMPARISONS WITH THE ACI METHOD

Design on the basis of a nonlinear calculation of the load-deflection relation and construction of the column interaction diagram is recommended by the ACI Build-  
ACI Structural Journal / July-August 1991

ing Code.<sup>1</sup> This code, however, permits the use of a simple approximate formula based on the magnification factor  $\gamma$

$$\gamma = \frac{C_m}{1 - \frac{P}{\phi P_c}} \geq 1.0 \quad (17)$$

in which  $P$  = axial load,  $\phi$  = strength reduction factor (0.70 for tied columns),  $P_c = \overline{EI} \pi^2/L^2$  where  $L$  = effective column length,  $\overline{EI}$  = effective bending stiffness of the column cross section, and  $C_m$  = correction coefficient that takes into account the initial bending mo-

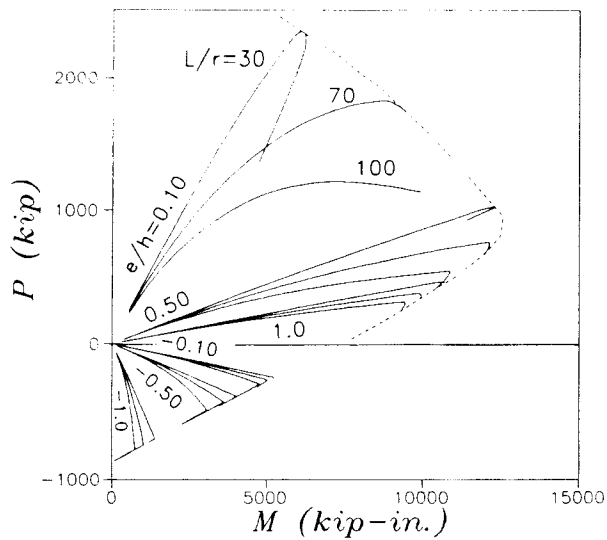


Fig. 7 — Load-versus-moment diagram as it extends into tension side

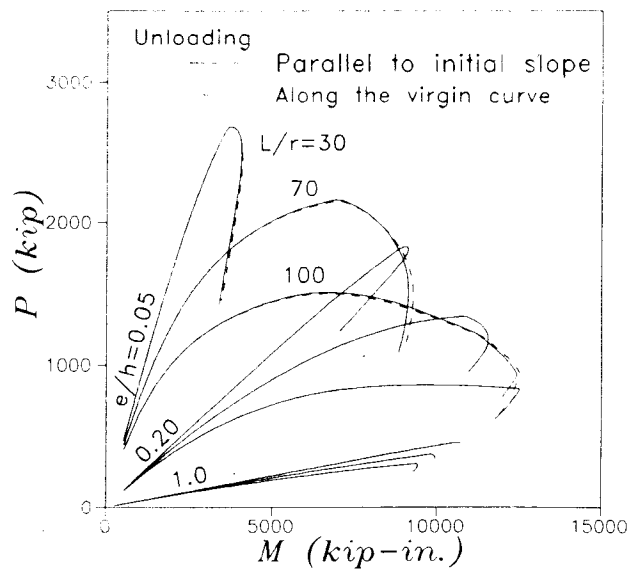


Fig. 9 — Load-versus-moment curves showing the effect of unloading

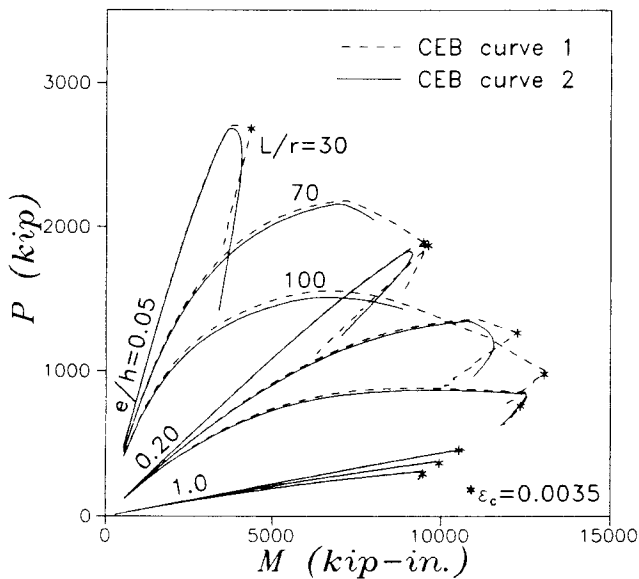


Fig. 8 — Load-versus-moment curves calculated for the two stress-strain curves recommended by CEB

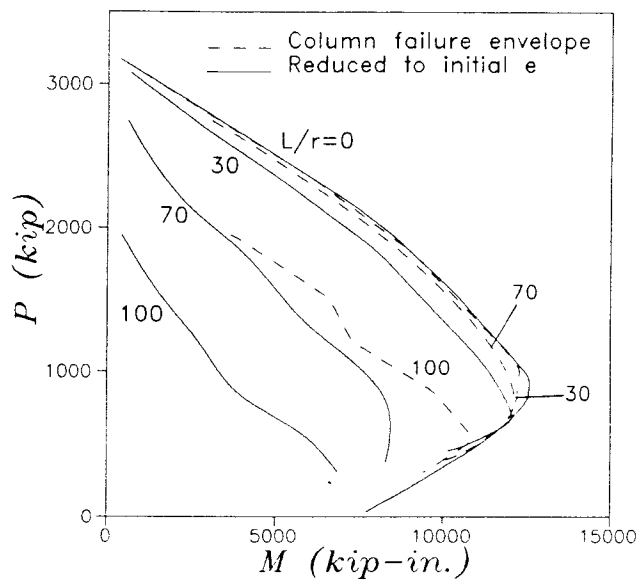


Fig. 10 — Column failure envelopes and reduced failure envelopes calculated for  $L/r = 30, 70, \text{ and } 100$

ment distribution along the column and the type of supports;  $C_m = 1$  for this example.

The effective bending stiffness for calculating  $P_c$  in Eq. (17) is allowed by the ACI Building Code to be estimated from the empirical equation

$$\bar{EI} = \alpha E_c^0 I_c^0 + \beta E_s^0 I_s \quad (18)$$

in which the long-time creep effects are neglected,  $I_c^0$  = gross moment of inertia of concrete cross section, and  $\alpha = 0.2$ . The coefficient  $\beta$  does not exist in the ACI Building Code and is inserted here for convenience, with the value  $\beta = 1.0$ . The value  $\alpha E_c^0$  is intended to give a conservative estimate of the secant modulus and thus takes into account the effect of nonlinearity of the moment-curvature diagram which is due mainly to concrete cracking.

It is interesting to compare  $\alpha$  and  $\beta$  with the coefficients  $\alpha_r$ ,  $\beta_r$  that correspond to  $P_r$  and the coefficients  $\alpha_i$ ,  $\beta_i$  that correspond to  $P_i$ . Eq. (8) gives  $\alpha_r = (E_c' I_c / E_c^0 I_c^0)$  and  $\beta_r = E_s' / E_s^0$ , while Eq. (14) gives  $\alpha_i = (\Phi_c I_c / I_c^0)$  and  $\beta_i = \Phi_s$ . Plotting these results in Fig. 11, we may conclude that Eq. (18) is not conservative for columns of small eccentricity for which  $L/r < 60$ . The same conclusion may be reached in yet another way;  $P_r$  requires calculating the bending stiffness from the tangent modulus, but this modulus gives a smaller bending stiffness than that given by Eq. (18), which roughly corresponds to the secant slope for the peak-moment point (Fig. 12).

ACI Eq. (17) includes a strength reduction by factor  $\phi$ , due to the inevitable random variability of the material. In the present formulation, however, this effect has not been incorporated. Thus, to make a compari-



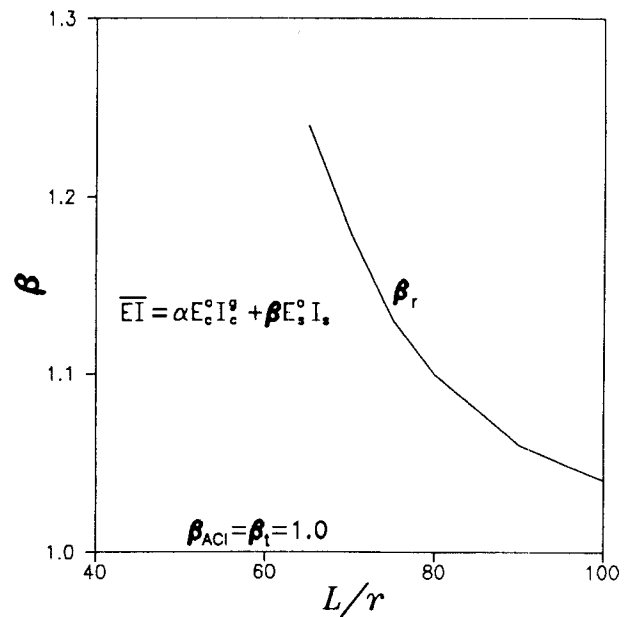
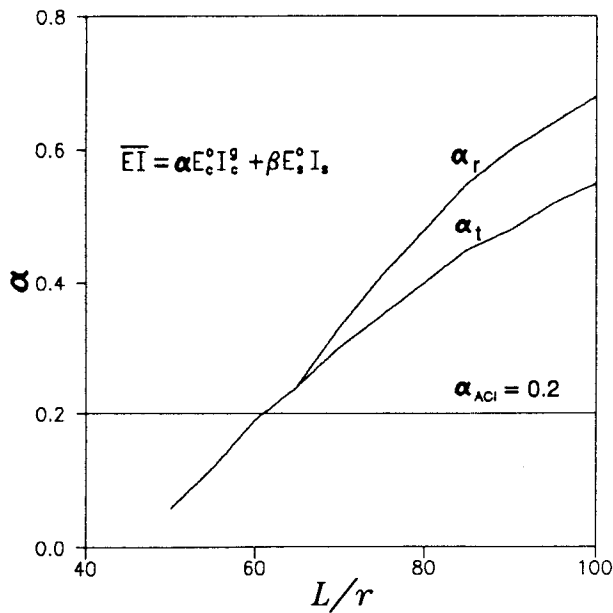


Fig. 11 — Coefficients multiplying the effective bending stiffnesses as given by ACI,  $P_t$  analysis, and  $P_t$  analysis

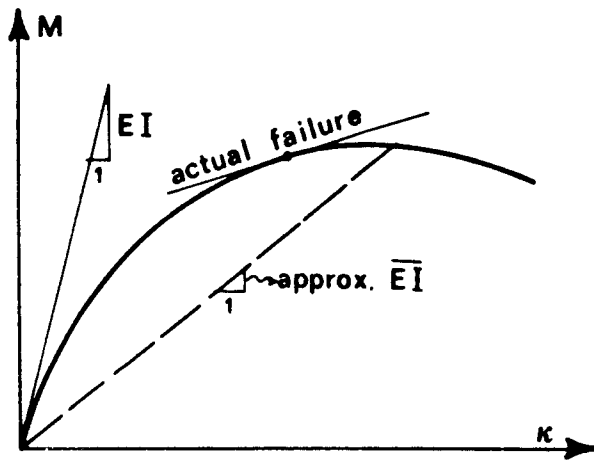


Fig. 12 — Moment-versus-curvature curve

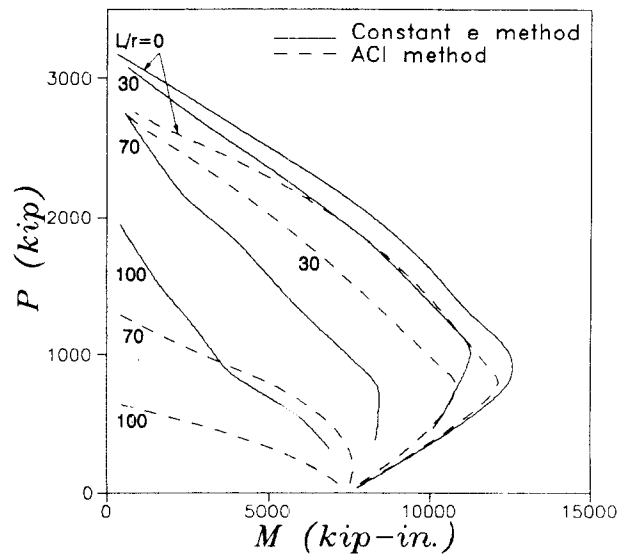


Fig. 13 — Reduced failure envelopes calculated according to the constant  $e$  method and the ACI method

son, either the factor  $\phi$  must be removed from Eq. (17) (i.e.,  $\phi = 1.0$ ) or a statistical reduction of material properties must be implemented in the present formulation.

The first type of comparison is the simplest, as well as clearest. The reduced interaction diagrams for  $L/r = 30, 70,$  and  $100$  are then obtained from the cross-sectional interaction diagram ( $L/r = 0$ ) by dividing the moment value by the corresponding  $\gamma$ -value given by Eq. (17) with  $\phi = 1.0$ . This yields the dashed curves interaction diagrams shown in Fig. 13. As one can see, the ACI method appears to be very conservative for the column we analyzed, except for small slenderness and large eccentricities.

#### COMPARISON WITH THE CEB METHOD

Instead of using the  $P(M)$  interaction diagrams, CEB recommends predicting the column response from the moment-curvature relations for various constant values

of the axial force.<sup>2</sup> The CEB Model Code permits the use of the so-called "model column method." This method is based on the approximate Eq. (4), which applies to a free-standing column [Fig. 14(a)]. The CEB model column method considers the plots of the applied moment and of the resisting moment versus curvature  $\kappa$  at the constant  $P$  [Fig. 14(b)]. The plot of applied moment  $M = M_t + M_{II}$  versus  $|\kappa|$  is, according to Eq. (4), an inclined straight line of slope  $P\kappa_{II}$ . This line may intersect the associated resisting  $M(\kappa)$  diagram at two points, at one point, or none. If there is no intersection, there exists no equilibrium state and the column fails dynamically. If there are two intersection points, such as Points 5 and 6 in Fig. 14(b), then Point 5 is stable (because at that point the resisting  $M$  increases faster than the applied  $M$ ), while Point 6 is unstable. The maximum  $P$  for which a stable state exists

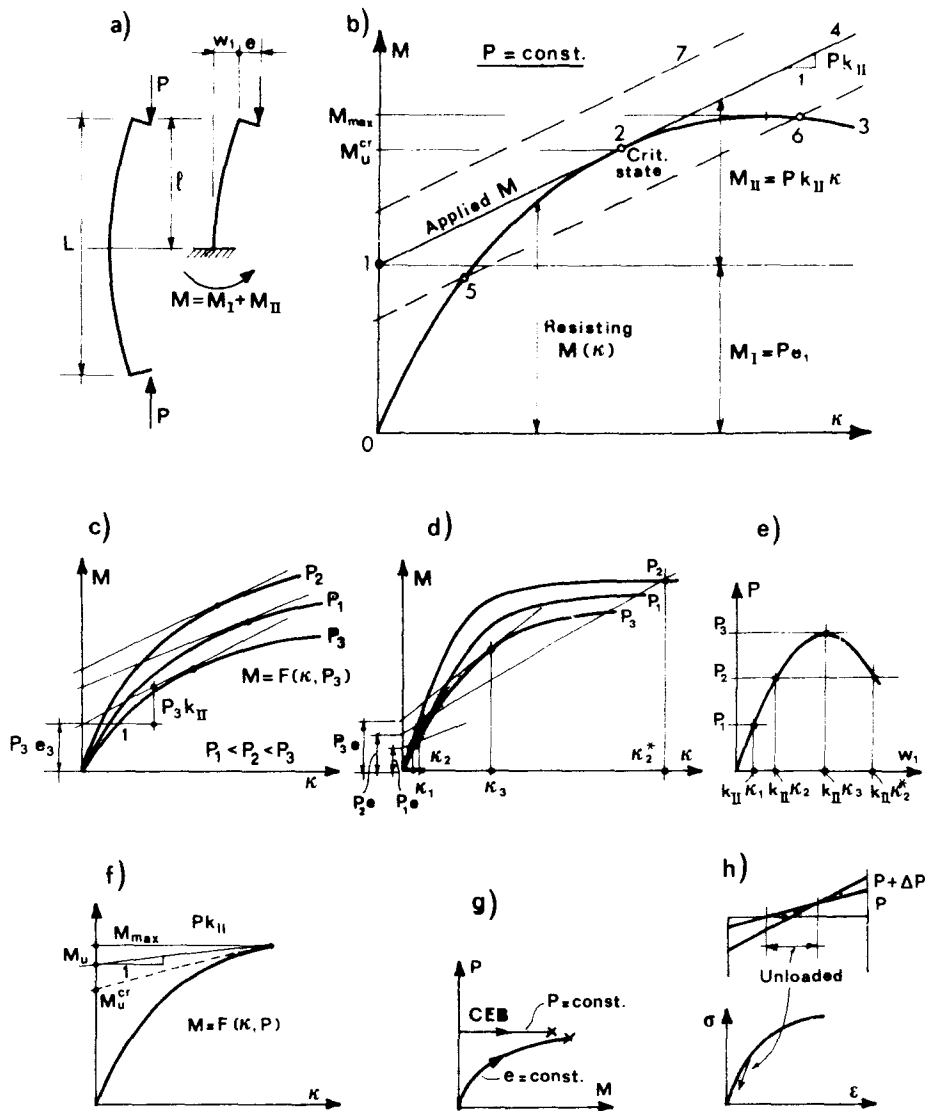


Fig. 14 — (a) Free standing model column; (b) moment-versus-curvature plot showing the resisting and applied moments defined according to the CEB model column method; (c) moment-versus-curvature curves for various  $P$ -values with tangents to the curves defining failure points; (d) moment-versus-curvature curves for various  $P$ -values intersected by straight lines representing equilibrium points; (e) load-versus-deflection curve obtained from the points of intersection shown in (d); (f) moment-versus-curvature curve ending at the limit compression strain of 0.0035 prescribed by CEB; (g) loading paths for constant  $e$  and constant  $P$ ; (h) unloading as it occurs with increasing load  $P$

occurs when the inclined straight line of applied  $M$  is tangent to its associated  $M(\kappa)$  diagram; see Line  $\bar{1}24$ .

The failure envelope for a column of given length (or slenderness) is determined according to CEB by selecting a number of constant  $P$ -values. For each of them, one calculates the  $M(\kappa)$  diagram  $\bar{0}3$  [Fig. 14(b)]. The tangent line  $\bar{1}24$  having slope  $Pk_{II}$  is then determined either graphically or by solving the  $\kappa$ -value for the tangent point from the nonlinear equation  $Pk_{II} = \partial M(\kappa) / \partial \kappa$ . The tangent point (Point 2) yields the ultimate bending moment for the critical state  $M_U^{cr}$ . The point  $(M_U^{cr}, P)$  is shown in the  $P(M)$  diagram as Point 3 in Fig. 3(f). The collection of all such points obtained for various  $P$ -values yields the failure envelope  $\bar{2}34$  [Fig. 3(f)] for the total  $M = M_I + M_{II}$  at failure. For design, however, it is more convenient to determine from Fig.

14(b) the value of the primary moment  $M_I$  corresponding to the tangent point 2 [ $M_I = \text{Segment } \bar{0}1$  in Fig. 14(b)]. In the  $P(M)$  diagram, the point  $(M_I, P)$  is shown as Point  $A_1$  [Fig. 3(f)], and it represents the horizontal projection of the failure point onto the radial ray of slope  $P/M_I = 1/e$ .

The determination of the case for which the applied restraining  $M(\kappa)$  curves are tangent is equivalent to solving  $P$  and  $\kappa$  from two simultaneous nonlinear equations

$$M_I + Pk_{II} \kappa = F(\kappa, P), \quad Pk_{II} = \partial F(\kappa, P) / \partial \kappa \quad (19)$$

where function  $F(\kappa, P)$  represents the resisting moment-curvature diagram  $M(\kappa)$  for any constant value  $P$ , as sketched in Fig. 14(c). The solution of Eq. (19) with a

standard computer library subroutine is a trivial matter once function  $F(\kappa, P)$  has been formulated.

The load-deflection curve for a fixed value of end eccentricity  $e$ , whose direct calculation we already explained [Eq. (5)], can also be constructed on the basis of the CEB model column method, provided that the effect of unloading a part of the cross section on the loading path is neglected. To this end, one needs to determine the intersections of the curves  $M = F(\kappa, P)$  with the straight lines  $M = Pe + k_{11}P\kappa$  representing the equilibrium values of the applied moment [Fig. 14(d)], and then calculate the corresponding deflection  $w_1 = k_{11}\kappa$ . Connecting these intersection points yields the load-deflection curve [Fig. 14(e)].

Note that the CEB model column method is applicable also for the case in which the failure is assumed to occur if the compression strain reaches 0.0035, while at the same time  $dP/dM > 0$  [Fig. 14(f)]. For a smaller value of the slope of the applied moment line, one finds a larger  $M_u$ , and as this slope approaches zero,  $M_u$  approaches the peak moment representing the cross-sectional strength.

The assumptions that the deflection curve is sinusoidal and that equilibrium needs to be insured only at the column midlength [Eq. (4)], are the same as those employed by the solution algorithm based on Eq. (7). The results must then be the same if the effect of unloading is neglected; see Fig. 15. The CEB model column method, however, cannot reproduce unloading in a meaningful way, since the  $M(\kappa)$  diagram is calculated at constant  $P$  (and variable  $e = M/P$ ) and thus does not represent the actual path followed by columns (whose loading is normally closer to that at constant  $e$ ); see Fig. 14(g). Although the effect of unloading has been found to be small, the constant  $e$  method proposed here is simpler and easier to use than the model column method because it does not require the construction of the  $M(\kappa)$  curves and the determination of the tangents to these curves.

### CONCLUSIONS

1. The column failure may be defined for design purposes as the peak of the diagram of axial load versus midlength bending moment at constant load eccentricity. This can be easily computed by a simple incremental loading algorithm with prescribed small increments of curvature at column midlength.

2. The tangent modulus load is approximately equal to the peak load of a column with load eccentricity 0.01 of cross-sectional thickness and represents a lower bound for the maximum load for still smaller eccentricities. Thus the tangent modulus load calculation could be used as an upper bound on column capacity, replacing the current ACI Building Code requirement for minimum eccentricity, which appears to be very conservative.

3. Strain irreversibility at unloading of portions of the cross section due to shifting of the neutral axis towards the compressed face can be easily taken into account, but its effect appears to be very small.

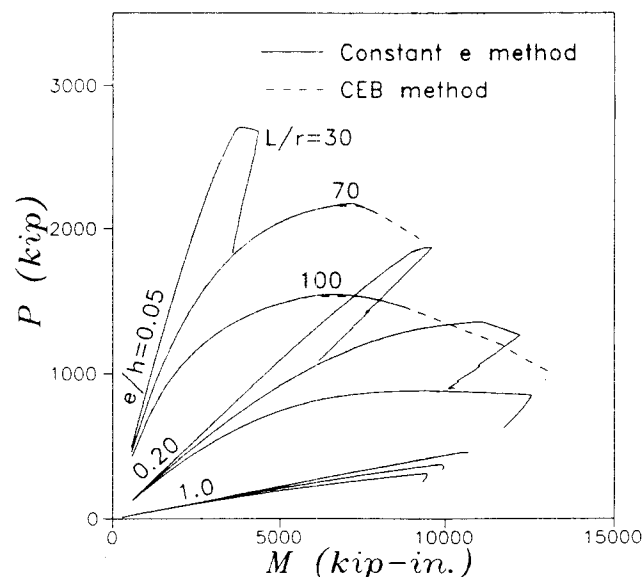


Fig. 15 — Load-versus-moment curves calculated for the constant  $e$  method and the CEB model column method

4. The proposed new method agrees well with the CEB method based on moment curvature relations of the cross section at constant axial load, but is simpler. In comparison to the ACI method, which is the simplest of all, there are large discrepancies.

5. Although sophisticated computer methods will play an increasingly important role and will become standard for the final check of design, there will be continuing need for a simple approach that offers insight into the column behavior.

### ACKNOWLEDGMENT

Partial support from the NSF Center for Advanced Cement-Based Materials at Northwestern University is gratefully acknowledged.

### CONVERSION FACTORS

1 in. = 25.4 mm  
 1 kip = 4448.2 N  
 1 kip-in. = 0.113 kN-m  
 1 kip/in.<sup>2</sup> = 6.9 MPa

### REFERENCES

1. ACI Committee 318, "Building Code Requirements for Reinforced Concrete and Commentary (ACI 318-89/318R-89)." American Concrete Institute, Detroit, 1989, 353 pp.
2. CEB-FIP Manual of Buckling and Instability, Comité Euro-International de Béton and Federation Internationale de la Précontrainte, Construction Press, Lancaster, 1978, 135 pp.
3. "CEB-FIP Model Code—First Predraft," Bulletin d'Information No. 190a, Comité Euro-International de Béton, Lausanne, July 1988.
4. Bažant, Z. P., and Cedolin, L., *Stability of Structures*, Oxford University Press, New York, 1991.
5. MacGregor, James G.; Breen, John E.; and Pfrang, Edward O., "Design of Slender Concrete Columns," ACI JOURNAL, Proceedings V. 67, No. 1, Jan. 1970, pp. 6-28.
6. Shanley, F. R., "Inelastic Column Theory," *Journal of Aerospace Science*, V. 14, No. 5, 1947, pp. 261-268.